

Soliton microcomb-assisted microring photonic thermometer with ultra-high resolution and broad range

CHENG ZHANG,^{1,2,†} JIN WANG,^{1,†} GUO GUO KANG,² JIANXIN GAO,^{1,3} ZHIER QU,^{1,2} SHUAI WAN,^{4,5} CHUNHUA DONG,^{4,5}  YIJIE PAN,^{1,6}  AND JIFENG QU^{1,7}

¹Center for Advanced Measurement Science, National Institute of Metrology, Beijing 100029, China

²School of Optics and Photonics, Beijing Institute of Technology, Beijing 100081, China

³College of Optical and Electronic Technology, China Jiliang University, Hangzhou 310018, China

⁴CAS Key Laboratory of Quantum Information, University of Science and Technology of China, Hefei 230026, China

⁵CAS Center for Excellence in Quantum Information and Quantum Physics, University of Science and Technology of China, Hefei 230026, China

⁶e-mail: panyijie@nim.ac.cn

⁷e-mail: qujf@nim.ac.cn

[†]These authors contributed equally to this work.

Received 1 June 2023; revised 16 July 2023; accepted 21 July 2023; posted 28 July 2023 (Doc. ID 496232); published 21 September 2023

Whispering gallery mode resonators (WGMRs) have proven their advantages in terms of sensitivity and precision in various sensing applications. However, when high precision is pursued, the WGMR demands a high-quality factor usually at the cost of its free spectral range (FSR) and corresponding measurement range. In this article, we propose a high-resolution and wide-range temperature sensor based on chip-scale WGMRs, which utilizes a Si_3N_4 ring resonator as the sensing element and a MgF_2 -based microcomb as a broadband frequency reference. By measuring the beatnote signal of the WGM and microcomb, the ultra-high resolution of 58 micro-Kelvin (μK) was obtained. To ensure high resolution and broad range simultaneously, we propose an ambiguity-resolving method based on the gradient of feedback voltage and combine it with a frequency-locking technique. In a proof-of-concept experiment, a wide measurement range of 45 K was demonstrated. Our soliton comb-assisted temperature measurement method offers high-resolution and wide-range capabilities, with promising advancements in various sensing applications. © 2023 Chinese Laser Press

<https://doi.org/10.1364/PRJ.496232>

1. INTRODUCTION

Chip-scale quantum metrology (CSQM) refers to those enabling technologies that offer self-validating and self-calibrated metrological standards and precision instruments that implement quantum effects on micro and nanoscale. For a chip-scale system, it is expected to consist of three layers. The foundation layer provides a high-stable laser source, the intermediate layer offers a broadband optical frequency reference for the readout process, and the top layer offers various functionalities to implement quantum standards and sensors. Significant efforts have been made in developing CSQM systems, including the integrated optical atomic clock [1], the chip-scale atomic magnetometer [2], and the photonic thermometer [3,4].

One of the focuses of CSQM research is the utilization of whispering gallery mode resonators (WGMRs) and their advantages in high-resolution sensing. Owing to the high Q -factor, small mode volume, high stability, and electromagnetic interference immunity, WGMRs are widely employed in precise measurements of temperature [5–8], humidity [9],

acoustic waves [10], displacement [11], stress/strain [12,13], and biological molecules [14,15]. Therefore, WGMRs can meet the demands of the top layer of the CSQM system for functionality. Although it is simple and convenient to integrate conventional WGMR-based devices, achieving high resolution and a wide dynamic range is still challenging. This limitation stems from the dependence of the measurement resolution on the frequency detection resolution, which is usually limited by the Q -factor of the WGMR. Assuming a constant fabrication-induced loss, it requires scaling up the size of the microcavity to enhance its Q -factor, by which it sacrifices the free spectral range (FSR) and the corresponding measurement range.

Despite the trade-off between the Q -factor and the FSR, readout technology is another aspect that influences the resolution and range of the sensor. In addition to the traditional wavelength scanning and peak-searching method, the side-of-fringe method detects power fluctuations when the pump frequency is fixed to the linear region of the resonance fringe [16]. While this method has achieved a resolution of 2.9 mK for

temperature sensing and less than 100 μK noise floor [16,17], its dynamic range is limited by the slope rate of the fringe, and the resolution is greatly affected by power and polarization disturbances. Another readout technique based on the pattern recognition method was proposed [18], which greatly enhances the measurement range by utilizing multi-mode rather than single-mode transmission spectra to eliminate the FSR limitation. However, the resolution is jointly limited by the precision of the recognition algorithm and frequency detection. Besides, acquiring the resonance frequency still requires laser scanning and a wavemeter, which limits the integration and response time of WGMR-based devices. Thirdly, the frequency-locking method, a promising readout technique, demonstrates higher resolution than other techniques by taking full advantage of the narrow linewidth characteristic of the WGM. The most proposed frequency-locking method-based WGM sensors were achieved by monitoring the measurand induced voltage response of the Pound–Drever–Hall (PDH) feedback signal [19–21]. However, the measurement range of conventional frequency-locking methods is limited by the linear region of feedback voltage, and environmental disturbances to the probe laser diode (e.g., vibrations) can induce additional feedback voltage variations, thereby increasing the outliers amount of readout data, which is detrimental to the accuracy.

The soliton microcomb is a promising optical frequency readout technique to solve the resolution and range trade-off issue in frequency-locking methods. This is due to the high coherence and low phase noise exhibited by soliton microcombs generated from high nonlinearity WGMRs [22], which make soliton microcombs well-suited for the optical frequency standard layer of CSQM systems. Recent studies have proposed chip-scale, high-resolution frequency measurement methods,

such as the Vernier microcombs-based wavemeter and repetition rate (f_{rep}) tuning microcomb-based wavemeter [23,24]. Although previous microcomb-based frequency measurement systems have achieved ultra-high-resolution frequency measurements, they primarily focused on spectroscopic measurements of gas-phase chemicals, without exploring other sensing applications, such as temperature sensing. Therefore, for sensing applications, there is an urgent need for a high resolution and wide range readout technique based on a single microcomb.

In this work, we propose a photonic thermometer that uses a soliton microcomb to achieve high-resolution and wide-range temperature sensing simultaneously. The laser frequency was locked to the resonance frequency of the Si_3N_4 microring via the PDH technique. And the temperature resolution of 58 μK was experimentally obtained by measuring the beatnote linewidth and sensitivity. A feedback voltage gradient based ambiguity resolving method was proposed to eliminate the non-ambiguous temperature range (NATR) caused by two symmetry beatnotes between comb-lines, which ensures the ultra-high resolution over the measurement range of 45 K, simultaneously. The present microcomb-assisted microring photonic thermometer realized high resolution and wide range, which holds significant potential for CSQM applications. As the first demonstration of a microcomb-based temperature sensor, our work showcases the vast prospects for the practical applications of optical microcombs [25].

2. PRINCIPLE

The proposed microcomb-assisted microring photonic thermometer consists of two primary devices: an on-chip microring and a high- Q microdisk, as shown in Fig. 1.

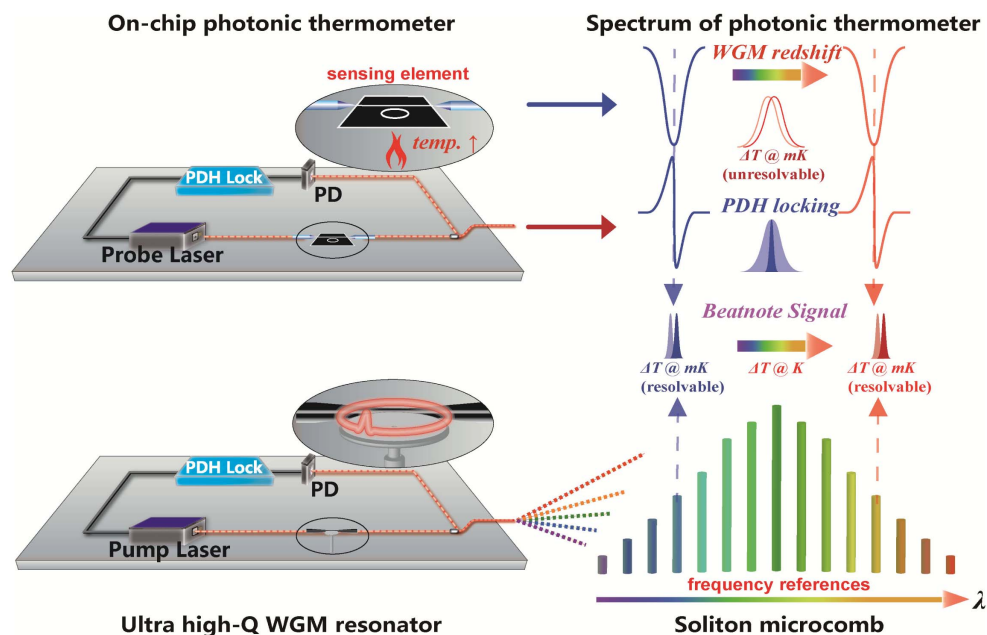


Fig. 1. Concept of the microcomb-assisted ultra-high-resolution and broad-range WGM photonic thermometer. The sensing element is an on-chip microring WGMR, which generates WGM red shift with increasing temperature (positive thermo-optic coefficient). The PDH locking ensures linewidth reduction and tracking of the WGM. The soliton microcomb provides broadband frequency references, thereby ensuring a broad range. By combining PDH-locking microring with a soliton microcomb, the temperature sensing achieves ultra-high resolution and broad range.

A. On-Chip WGMR-Based Photonic Thermometer

The on-chip WGMR is used as a micro-scale sensing element to measure small temperature variations of the object. The temperature variation ΔT of the measured object is transmitted from the chip substrate to the WGMR. And the frequency shift Δf of the WGM resonance can be monitored, which results from the combination of the thermo-optic effect and thermo-elastic effect of the WGMR material. As shown in Fig. 1, resonance redshift results from heating WGMR with positive thermo-optic coefficient $\partial n_{\text{eff}}/\partial T$, such as Si_3N_4 and Si. Therefore, the temperature-frequency sensitivity S of an on-chip WGMR-based photonic thermometer can be expressed as follows [26]:

$$S = \frac{\Delta f}{\Delta T} = -\frac{f}{n_g} \left(\frac{\partial n_{\text{eff}}}{\partial T} + \frac{n_{\text{eff}}}{L} \frac{\partial L}{\partial T} \right), \quad (1)$$

where n_g , n_{eff} are the group index and the effective index of WGMR respectively, and L is the perimeter of WGMR. Note that the thermo-refractive effect induced frequency shift Δf is typically greater than the thermo-elastic effect.

Considering both the instrumental resolution and the FWHM is crucial for determining the resolution Δf_{scan} of the conventional frequency scanning method. In line with the assumption made in Ref. [18], we adopt the corresponding resolution, denoted as $R_{\text{scan}} = \frac{\Delta f_{\text{scan}}}{|df/dT|} = \frac{\Delta f_{\text{FWHM}}}{10|S|}$ [26]. The frequency-locking methods, such as PDH technique and self-injection locking, can effectively break through the limitation of the WGM linewidth Δf_{FWHM} since the laser linewidth Δf_{lock} can be narrowed down to 1/1000 to 1/10,000 of the Δf_{FWHM} [27–30]. Assuming $\Delta f_{\text{lock}} = \Delta f_{\text{FWHM}}/1000$, the frequency-locking methods lead to an ultra-high measurement resolution R_{lock} by [26]

$$R_{\text{lock}} = \frac{\Delta f_{\text{lock}}}{|S|} = \frac{\Delta f_{\text{FWHM}}}{1000|S|} \ll \frac{\Delta f_{\text{FWHM}}}{10|S|} = R_{\text{scan}}. \quad (2)$$

B. Microcomb-Based Readout Technique

By utilizing the balance of gain, loss, dispersion, and nonlinearity of the high- Q WGMR, combined with dispersion engineering [31,32], a soliton microcomb with high stability and specific repetition frequency f_{rep} can be generated. The temperature variation of the on-chip WGMR leads to the resonance frequency shift that is converted into the radio-frequency (RF) frequency shift of the microcomb-WGM (MC-WGM) beatnote f_b between comb-lines $f_{m,m+1}$ ($f_m = f_{\text{ceo}} + mf_{\text{rep}}$, where f_{ceo} is the carrier envelope offset frequency) and frequency-locked probe laser f_{lock} .

As shown in Fig. 2, the beating between the comb-lines and probe laser generates two symmetrical spacing beatnote RF signals f_b and $f_{\text{rep}} - f_b$, which results in the NATR ($T_{\text{NATR}} = f_{\text{rep}}/2S$). Note that the NATR is in the frequency domain, which is similar to the non-ambiguous range (NAR) of ranging applications in the time domain [33]. When measuring temperature larger than the NATR, a crucial consideration is to count the integer multiple of the NATR to accurately obtain the real temperature T_r using [33]

$$T_r = T_0 + N \frac{f_{\text{rep}}}{2S} \pm \frac{f_b}{S}, \quad (3)$$

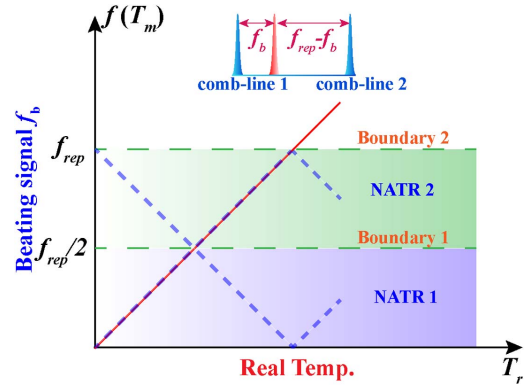


Fig. 2. Beatnote ambiguity during microcomb-assisted temperature sensing. The blue dashed line, red solid line, and green dashed line are the beatnote signals, real temperature curve, and non-ambiguous temperature range (NATR) boundary, respectively.

where N is the integer multiple and T_0 is the initial temperature offset, which is obtained by the initial probe laser frequency and its nearest comb-line at initial actual temperature $T_{r,0}$ as $T_0 = T_{r,0} \pm f_{b,0}/S$. Note that the sign of f_b/S is determined by N , where “+” is for positive even integers and negative odd integers N and vice versa.

In order to readout integer multiple N of NATR by tracking the target beatnote signal f_b , we proposed the gradient of the feedback voltage to resolve the beatnote ambiguity. The basic principle relies on the fact that the ambient temperature-induced resonance frequency shift results in the voltage variation of the PDH feedback signal, as the PDH loop compensates for the frequency shift in real time. Therefore, the actual temperature gradient and corresponding beatnote frequency gradient can be obtained by monitoring the voltage gradient of the PDH feedback signal, which can be derived by calculating the gradient of Eq. (3) as

$$\begin{aligned} \partial_t T_r &= \partial_t (T_0 + N \cdot T_{\text{NATR}}) \pm \frac{1}{S} \partial_t f_b \\ &= 0 \pm \frac{1}{S} \partial_t f_b \propto -\frac{\partial V_{\text{FB}}}{\partial t}. \end{aligned} \quad (4)$$

Note that the relationship between the feedback voltage gradient and actual temperature gradient is inversely proportional, which is obtained by pre-calibration.

Finally, the integer multiple N and real-temperature T_r can be obtained as follows.

- (i) Set the integer multiple $N = 0$ at the start of the measurement.
- (ii) Measure the nearest comb-line and $T_{r,0}$ using the pre-calibrated probe laser and beatnote frequency $f_{b,0}$ since the microcomb is generated with a fixed pump.
- (iii) Reconstruct the measured beatnote f_b and count N by comparing the sign of the beatnote frequency f_b and feedback voltage, according to Eq. (4).
- (iv) Use Eq. (3) to obtain the actual temperature T_r since f_b is measured; $T_{r,0}$, $f_{b,0}$ are pre-calibrated in step (ii), and N is counted in step (iii).

Moreover, the microcomb frequency noise can induce additional measurement uncertainty, which is detrimental to the accuracy. Considering $f_m = f_{\text{ceo}} + mf_{\text{rep}}$, the measurement uncertainty ΔT_r can be obtained by measuring the frequency stability of comb-line f_m by using

$$\begin{aligned} \Delta T_r &= \frac{\Delta f_m}{|S|} = \frac{1}{|S|} \sqrt{\Delta f_{\text{ceo}}^2 + (m\Delta f_{\text{rep}})^2} \\ &= \frac{1}{|S|} \sqrt{\Delta f_{\text{pump}}^2 + [(m - m_{\text{pump}})\Delta f_{\text{rep}}]^2}, \end{aligned} \quad (5)$$

where Δf_{pump} is the pump frequency stability.

3. FABRICATION AND EXPERIMENTAL SETUP

A. Fabrication of WGMRs

For on-chip photonic thermometry, we fabricated a microring resonator on a $0.8 \mu\text{m}$ Si_3N_4 film, which is grown on the wafer with a $3 \mu\text{m}$ buried SiO_2 layer and a $500 \mu\text{m}$ silicon substrate. To mitigate cracking in thick Si_3N_4 film, we utilized a diamond scribe and lithography with buffered oxide etch to create trenches. We deposited the film in 400 nm steps and performed post-annealing at 1100°C to reduce absorption loss and relieve tensile stress [34]. Its scanning electron microscope (SEM) image is shown in Fig. 3(a). The radius of the microring is $100 \mu\text{m}$, the cross section is $1.8 \mu\text{m} \times 0.8 \mu\text{m}$, and the gap between the microring and the bus waveguide is 300 nm . We also characterized the fundamental TE mode of Si_3N_4 microring with the

loaded- Q of 4.75×10^5 , the FSR of 228.8 GHz , and the temperature sensitivity of $S = -2.3 \text{ GHz/K}$ [35].

For high stability single-soliton microcomb generation, we fabricated a MgF_2 microdisk resonator using the semi-automated precision grinding and polishing process [36]. As shown in Fig. 3(b), the total radius of the fabricated MgF_2 microdisk is 4.67 mm , and the sidewall thickness is about $400 \mu\text{m}$. The measured intrinsic Q -factor of the MgF_2 microdisk is greater than 9×10^9 , which has an extremely low four-wave mixing threshold power at mW-level. The MgF_2 microdisk has high temperature stability and a repetition rate of about 7.5 GHz due to its millimeter-scale, which makes the generated MC-WGM beatnote signal more stable and easily meets the requirements of most photodetectors (PD) in bandwidth.

B. Soliton Microcomb Generation and MC-WGM Beatnote Characterization

The MC-WGM beatnote temperature measurement system is shown in Fig. 3(d), which consists of a soliton microcomb and a microring-based photonic thermometer. Each module adopts PDH technique to obtain long-term stable single soliton microcombs and optical frequency signals, respectively. In addition, RF synthesizers and other RF devices such as the real-time spectrum analyzer (RSA) are referenced to a 10 MHz frequency reference derived from a commercial rubidium atomic clock.

In the soliton microcomb generation module, we used AWG1 (Keysight, 33500B) to control ECDL1 (Toptica, CTL1550) to scan the fundamental TE mode near 193.402 THz . The pump

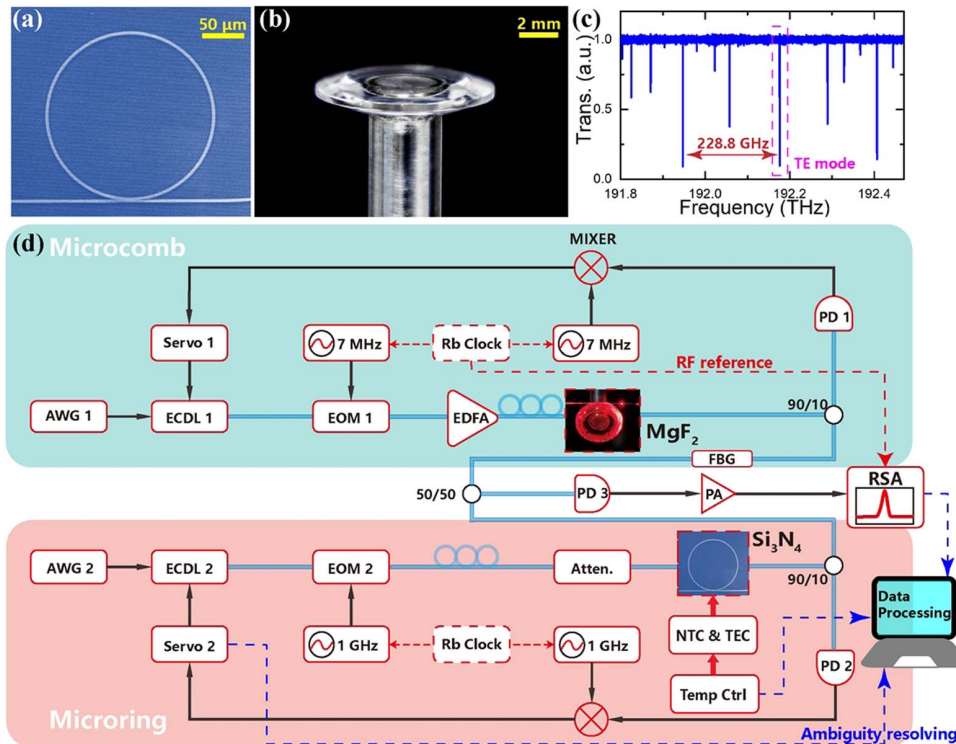


Fig. 3. (a) SEM image of fabricated Si_3N_4 microring resonator; (b) image of fabricated MgF_2 microdisk resonator; (c) measured transmission spectrum of Si_3N_4 microring resonator; (d) experimental setup of microcomb-assisted temperature sensing system: AWG, arbitrary waveform generator; ECDL, external-cavity diode laser; EOM, electro-optic modulator; EDFA, erbium-doped fiber amplifier; PD, photodetector; FBG, fiber Bragg grating; PA, preamplifier; RSA, real-time spectrum analyzer; NTC, negative temperature coefficient thermistor; TEC, thermoelectric cooler; Atten., attenuator.

field was amplified by an EDFA to 350 mW and then coupled into the MgF_2 microdisk through a tapered fiber with a total loss of 1.5 dB, and the transmission spectrum with soliton steps was obtained. Before coupling into microcavity, the pump light was phase modulated using EOM1 to generate the PDH error signal. The PDH feedback signal of the MgF_2 microdisk is then fed back to the ECDL1 current through servo1 to lock on the single soliton step. In addition, we also used a programmable thermoelectric cooler (TEC) controller to precisely control the temperature of the sealed MgF_2 microdisk at the mK level, further improving the stability of the generated single soliton microcomb.

In the photonic thermometer module, the probe light of 192.176 THz was coupled into the bus waveguide by edge coupling through a lensed fiber at room temperature. By scanning the fundamental TE mode and using the PDH feedback loop to control the currents, piezoelectric ceramic transducer (PZT), and motor voltage of ECDL2, the probe laser can be locked on the WGM resonance, and a well-maintained stable optical frequency signal is obtained. The motor voltage feedback ensured that the ECDL2 is continuously locked within a wide temperature range. Since the FWHM of the Si_3N_4 resonance is 400 MHz, the EOM modulation frequency is set to 1 GHz. To precisely control the temperature of Si_3N_4 microring, we used a temperature controller (SRS, LDC501) and a waveguide holder (Suruga Seiki, F274-18) with a pre-calibrated negative temperature coefficient (NTC) thermistor and TEC. Note that the maximum TEC temperature tuning step is 1 K due to the current limitation. In addition, the intracavity power was reduced by an attenuator to minimize the self-heating induced temperature deviation on temperature measurement [35]. The temperature controller and monitor were also remotely controlled by a PC to read the device's temperature with a sampling time of 0.2 s. Note that both the temperature control and monitoring resolution are 1 mK. Furthermore, we insulated the Si_3N_4 microring with a 3D-printed protective cover that includes thermal insulation layers to minimize convective heat transfer, which is detrimental to sub-mK-level temperature measurements.

Finally, two optical paths including the soliton microcomb and microring-based photonic thermometer were combined at a 50/50 coupler and were detected by a 12 GHz bandwidth PD (Newport, 1544-B). The RF beatnote signal was sent to a remote-controlled real-time spectrum analyzer (Rigol, RSA3030-TG) and a PC readout the RF spectrum with a sampling time of 0.3 s. In addition, we transmitted the PDH feedback signal

of the Si_3N_4 microring to the PC. And by monitoring the gradient of the feedback voltage, we performed beatnote ambiguity resolving at the NATR boundary, thereby improving the dynamic range of temperature measurement.

4. RESULTS

To experimentally verify the capability of the proposed microcomb-assisted photonic thermometer, we performed MC-WGM beatnote characterization, signal ambiguity resolving near the NATR boundary, and high-resolution temperature measurements in a broad range.

A. Soliton Microcomb Generation and MC-WGM Beatnote Characterization

The proposed microcomb-assisted photonic thermometer was first operated at well-maintained room temperature ($T_{r0} = 294.65$ K). As shown in Fig. 4(a), we used the offset-PDH locking technique to generate a long-term stable single-soliton microcomb [37], which has a smooth sech^2 envelope with a repetition rate f_{rep} of 7.47 GHz and a -3 dB bandwidth (-3 dB-BW) of 1.2657 THz. The -3 dB-BW is significantly larger than the FSR of the Si_3N_4 microring, indicating that our method can surpass the limitation imposed by the sensing element's FSR. Considering the temperature sensitivity ($S = -2.3$ GHz/K) of the Si_3N_4 microring, the derived theoretical measurement range is -3 dB-BW/ $|S| = 550$ K. In addition, several dispersive waves (DWs) can be observed in microcomb spectra, which results from the mode crossing caused by the millimeter scale of MgF_2 cavity. Note that DW-induced power enhancement of the MC-WGM beatnote does not affect the resolution of beat frequency temperature measurement.

As shown in Fig. 4(b), we measured the MC-WGM beatnote at room temperature ($T_{r0} = 294.65$ K), which has a center frequency f_{b0} of 940.1 MHz, a signal-to-noise ratio (SNR) of 38 dB, and a -3 dB linewidth of 134 kHz. The temperature resolution of the generated beatnote was calculated to be 58 μK , indicating that the proposed method is capable of μK -level resolution measurements. In addition, there are ± 7 MHz beatnote sidebands with SNR < 10 dB, which result from the EOM modulated signal and do not affect the temperature measurement results.

To measure actual temperature T_r , we derived the initial temperature offset T_0 as follows. Since the initial probe laser frequency of 192.176 THz, the nearest comb-line can be derived to be 192.17506 THz ($f_0 = f_{\text{ceo}} + m f_{\text{rep}}$, $m = 25726$), and the integer multiple of NATR was set as $N = 0$. Thus, the

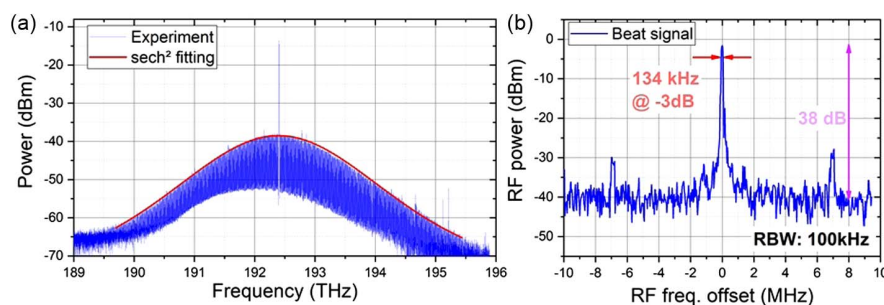


Fig. 4. (a) Optical spectrum of single-soliton microcomb; (b) electrical spectrum of MC-WGM beatnote signal.

initial temperature offset T_0 can be derived to be $T_0 = T_{r0} - f_{b0}/S = 295.062$ K. Therefore, by measuring the T_0 at initial actual temperature, and introducing ambiguity resolving method to count integer multiple N , the actual temperature T_r of sensing element can be measured by using Eq. (3).

B. Ambiguity Resolving near the NATR Boundary

To verify the effectiveness of the proposed signal ambiguity resolving method, we experimentally conducted temperature measurement near the NATR boundary, as shown in Fig. 5. We first controlled the temperature of Si_3N_4 microring to around 293.438 K (white dashed line) at the boundary of the NATR (integer multiple of NATR $N = 0$), making the target beatnote signal close to its symmetrical signal. Note that we down-mixed the MC-WGM beatnote signal to meet the RSA bandwidth requirements. The temperature of the Si_3N_4 microring continuously increases and decreases within 150 s, and the alternate MC-WGM beatnote signals can be observed on the measured spectrum, as shown in Fig. 5(a). As shown in Fig. 5(b), we synchronously acquired and solved the voltage gradient of the feedback signal, which is directly related to the temperature gradient in Figs. 5(a) and 5(c) by using Eq. (4). It is worth noting that the ambiguity of measured beatnote can be resolved in real time since the voltage sampling rate of 512 Hz is much faster than the beatnote sampling rate. As shown in Fig. 5(c), the reconstructed temperature curve is consistent with the actual temperature near the NATR boundary, which proves the effectiveness of the proposed ambiguity-resolving method that can track the target beatnote signal and readout integer multiple N .

C. Ultra-High Resolution Measurement in a Broad Range

We performed a proof-of-concept experiment to verify that the proposed temperature measurement method maintains ultra-high resolution over a wide dynamic range. As shown

in Fig. 6, the measured temperature range reached 45.15 K, and the temperature measurements with mK-level steps were carried out in room temperature, low-temperature ($N = 9$), and high-temperature ($N = -18$) regions respectively. The measured temperature is derived from the beatnote RF spectrum using Eq. (3), which can directly reflect real-time temperature variation. As shown in Figs. 6(b)–6(d), by comparing the measured temperature curves with the reference curves and calculating the standard deviation of readout data before the heating process, the proposed measurement method demonstrates an ultra-high resolution of 136 μK over a broad range of 45 K.

The deviation between the measured range and the reference range is 0.5 K, which is mainly due to the increment of convective heat transfer between the TEC and the microring in both the high and low-temperature regions. The temperature deviation exhibited positive and negative values in the low- and high-temperature regions, respectively, further validating the presence of convective heat transfer. Moreover, the temperature deviation curve reflects the heat transfer rate, causing the spikes of temperature difference between the microring and the TEC during each temperature rise, demonstrating the high response rate of the proposed sensor.

The resolution of 136 μK is limited by the RF frequency resolution at a sampling time of 0.3 s, and the range of 45 K is limited by the operating range of temperature controller. Note that our proposed method can maintain frequency locking over a wide range, and the MC-WGM beatnote crossed 28 comb-lines in the experiment, which indicates a broad range that is not limited by FSR but limited by comb-line spanning. The measured temperature profiles in each temperature region reflect proportion integration differentiation (PID) overshoot induced sub-mK oscillations during the heating process, further proving that the proposed temperature measurement method can maintain high resolution over a wide dynamic range.

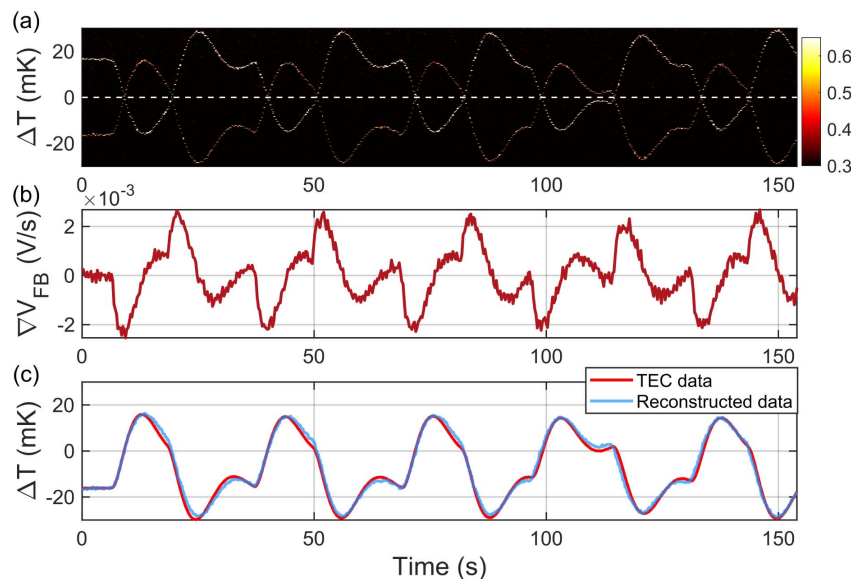


Fig. 5. (a) Measured waterfall spectrum shows signal ambiguity near the NATR boundary (white dash line); (b) measured voltage gradient of the feedback signal for ambiguity resolving process; (c) reconstructed temperature curve (blue solid line) and reference temperature curve (red solid line).

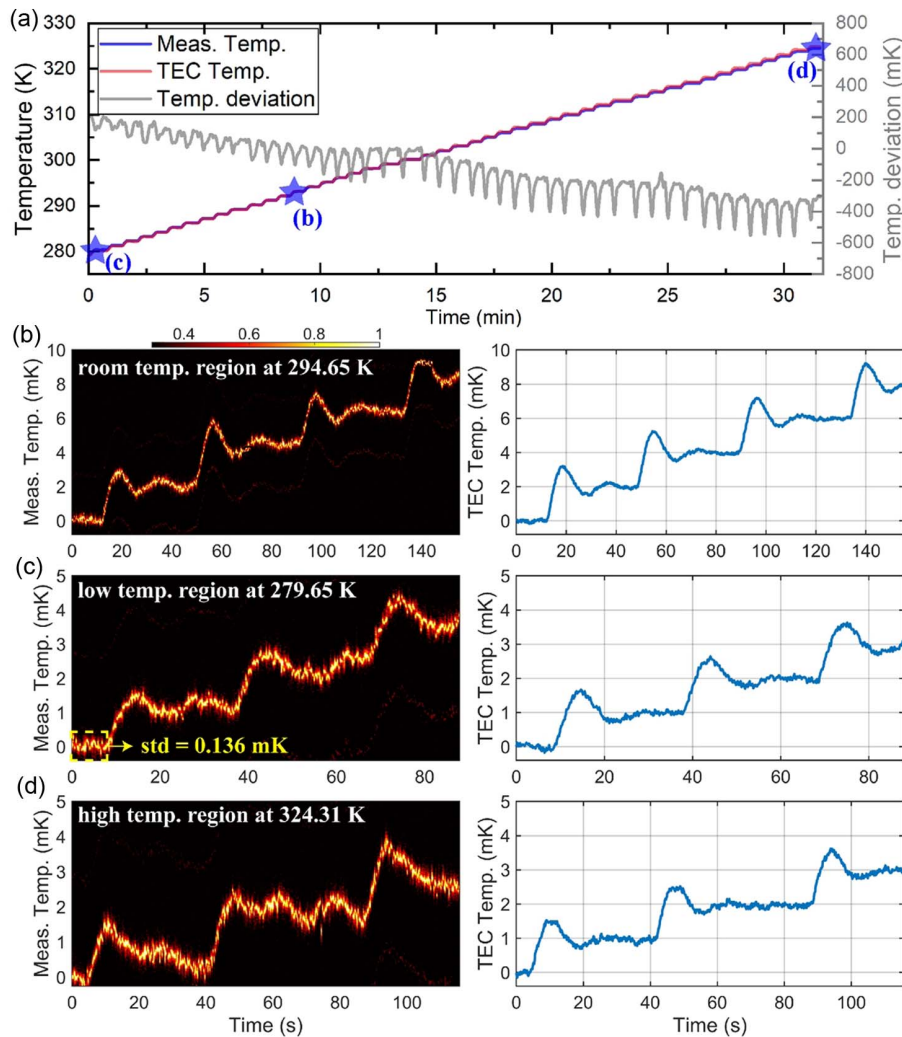


Fig. 6. (a) Measured temperature curve shows ultra-high resolution in a broad temperature range, and the temperature deviation curve reflects the heat transfer rate, proving our proposed sensor has a fast response (temp. deviation = meas. temp. - TEC temp.); (b)–(d) mK-level temperature measurement in various temperature regions proves the ultra-high resolution of 136 μ K.

5. DISCUSSION

To analyze the accuracy of our proposed measurement method, we further measured the temperature uncertainty caused by microcombs. Considering the effect of soliton microcomb detuning-locking method on measurement accuracy, we performed auxiliary mode locking and offset-PDH-locking at room temperature (294.65 K), respectively, as shown in Fig. 7(a). The auxiliary mode exploits the thermal equilibrium between the red-detuned soliton step of the pump mode and the blue-detuned of the higher-order mode to obtain a long-term locked microcomb without external active feedback [38,39]. It is worth noting that, although a higher-order mode exists at the soliton stage of the offset-PDH-locking spectrum, it has a negligible effect on the soliton thermal balance due to insufficient thermal broadening.

We measured the Δf_{rep} of the two detuning-locking methods using a frequency counter at a gate time of 0.1 s and obtained the Δf_{pump} by recording the pump frequency, as shown in Figs. 7(b) and 7(c). Results show that the temperature

uncertainty caused by Δf_{rep} of the offset-PDH-locking scheme is much smaller than that in the aux-mode-locking at a gate time of 0.1 s. The main reason for this difference is that the aux-mode-locking is based on passive locking with intracavity temperature compensation, while the pump light is still free-running, resulting in poorer temperature stability. Therefore, for high-resolution temperature measurement, the offset-PDH-locking scheme has higher accuracy. Assuming $m - m_{\text{pump}} = 500$, we calculated the offset-PDH-locked microcomb induced uncertainty using Eq. (5), which is 5.65 μ K at 0.1 s at room temperature, indicating that the accuracy of our proposed method reaches μ K-level. In addition, the generated microcomb can be well-maintained for several hours, and the long-term temperature stability is below 11.91 μ K at 100 s, which shows the proposed microcomb-assisted temperature measurement system has high repeatability and robustness.

As shown in Table 1, frequency-locking method-based photonic thermometers not only achieve the resolution that is higher

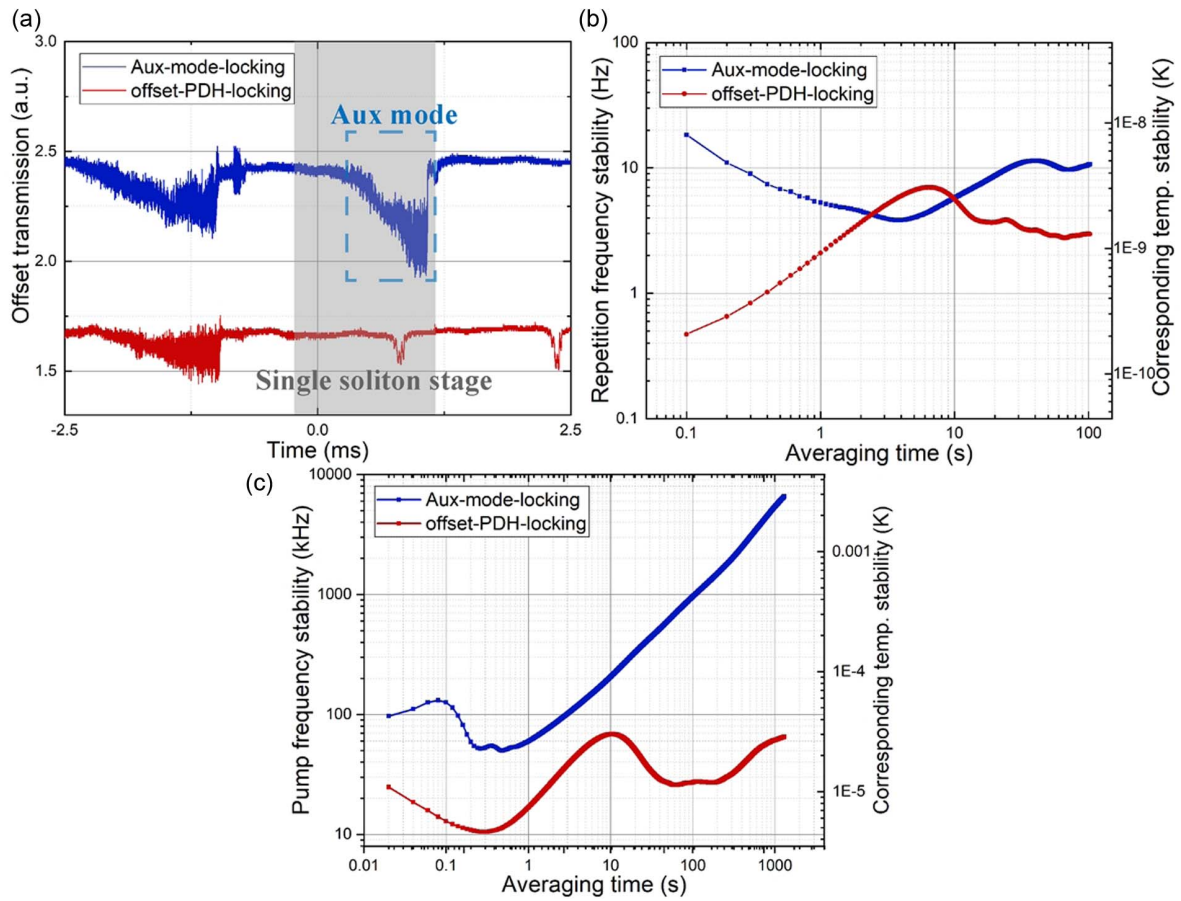


Fig. 7. (a) Transmission spectra of two different soliton locking regimes; (b) repetition frequency stability and corresponding temperature stability of two different soliton locking regimes; (c) pump frequency stability and corresponding temperature stability of two different soliton locking regimes.

Table 1. Comparison of Chip-Scale Photonic Thermometer Performance

Material	Structure	Resolution (mK)	Range Limited by FSR (K)	Readout Technique	Reference
Silicon	Microring	10.0	280	Frequency-scanning and peak-searching	[46]
Silicon	Microring	31.3	135	Frequency-scanning and peak-searching	[7]
Silicon	Microring	2.90	157	Frequency-scanning and side-of-fringe	[17]
Silica	Microbubble	40.0	Not limited by FSR ^a	Frequency-scanning and optical barcode	[18]
Silicon	Cascaded microrings	0.09	Not limited by FSR ^b	Frequency-locking and reference microring	[40]
Silicon nitride	Microring	0.058	Not limited by FSR ^c	Frequency-locking and microcomb	This work

^aLimited by original database range.

^bLimited by PD bandwidth.

^cLimited by comb-line spanning.

by two orders of magnitude than that of frequency-scanning-based thermometers but also eliminate the range limitation caused by FSR. Additionally, our proposed microcomb-based readout method ensures both ultra-high resolution and a broad range simultaneously when compared with the reference microring-based readout technique, which is limited by fast PD bandwidth [40]. The microcomb-assisted photonic thermometer does not require optical frequency calibration by a large-volume and high-precision wavelength meter, making it

more integrated and faster, which meets the requirements of high-resolution CSQM. In technical terms, the proposed ambiguity-resolving method overcomes the limitation of the dynamic range of MC-WGM beatnote sensing, which can expand the application of the MC-WGM beatnote sensing method. In material terms, using temperature-dependent thermo-optic coefficients [41,42] can further extend the dynamic range in cryogenic applications. In the future, by introducing heterogeneously integrated microcombs [43], integrated Sagnac

interferometers [44,45], and chip-scale atomic clocks, the proposed method can realize fully integrated, mass-producible, high-resolution, and wide-range photonic sensors.

6. SUMMARY

We proposed a novel sensing approach based on microcomb-based readout technique. Our approach leverages the microcomb-microring beatnote for temperature measurement of on-chip devices with an ultra-high resolution of 58 μK . Moreover, by utilizing feedback voltage gradient of the PDH-locked loop to resolve beatnote ambiguity at each NATR, the ultra-high temperature resolution and a broad range of 45 K were obtained simultaneously in the proof-of-concept experiment. By analyzing the frequency stability of the microcomb f_{rep} and f_{pump} , we deduced that the soliton comb-line frequency induced temperature uncertainty is 5.65 μK at 0.1 s, which ensures high accuracy of the proposed method. With its high-resolution and wide-range temperature measurement capabilities, our proposed method demonstrates its suitability for scientific and industrial applications.

Funding. National Key Research and Development Program of China (2022YFF0608304); National Natural Science Foundation of China (62075206, 62205324).

Acknowledgment. This work was partially carried out at the USTC Center for Micro and Nanoscale Research and Fabrication. The authors gratefully acknowledge the helpful discussions by Fei Meng and the valuable advice by Liuying Yan on manuscript preparation.

Disclosures. The authors declare no conflicts of interest.

Data Availability. Data underlying the results presented in this paper may be obtained from the authors upon reasonable request.

REFERENCES

- Z. L. Newman, V. Maurice, T. Drake, J. R. Stone, T. C. Briles, D. T. Spencer, C. Fredrick, Q. Li, D. Westly, B. R. Ilic, B. Shen, M.-G. Suh, K. Y. Yang, C. Johnson, D. M. S. Johnson, L. Hollberg, K. J. Vahala, K. Srinivasan, S. A. Diddams, J. Kitching, S. B. Papp, and M. T. Hummon, "Architecture for the photonic integration of an optical atomic clock," *Optica* **6**, 680–685 (2019).
- P. D. D. Schwindt, S. Knappe, V. Shah, L. Hollberg, J. Kitching, L.-A. Liew, and J. Moreland, "Chip-scale atomic magnetometer," *Appl. Phys. Lett.* **85**, 6409–6411 (2004).
- S. Dedyulin, Z. Ahmed, and G. Machin, "Emerging technologies in the field of thermometry," *Meas. Sci. Technol.* **33**, 092001 (2022).
- A. J. Fleisher, Z. Ahmed, T. Herman, and M. R. Hartings, "Dual electro-optic frequency comb photonic thermometry," *Opt. Lett.* **48**, 2210–2213 (2023).
- X. Xu, W. Chen, G. Zhao, Y. Li, C. Lu, and L. Yang, "Wireless whispering-gallery-mode sensor for thermal sensing and aerial mapping," *Light Sci. Appl.* **7**, 62 (2018).
- X. Zhang, Y. Yang, H. Bai, J. Wang, M. Yan, H. Xiao, and T. Wang, "Theoretical aspects and sensing demonstrations of cone-shaped in-wall capillary-based microsphere resonators," *Photon. Res.* **5**, 516–520 (2017).
- M. You, Z. Lin, X. Li, and J. Liu, "Chip-scale silicon ring resonators for cryogenic temperature sensing," *J. Lightwave Technol.* **38**, 5768–5773 (2020).
- C. Zhang, G. Kang, Y. Xiong, T. Xu, L. Gu, X. Gan, Y. Pan, and J. Qu, "Photonic thermometer with a sub-millikelvin resolution and broad temperature range by waveguide-microring Fano resonance," *Opt. Express* **28**, 12599–12608 (2020).
- A. K. Mallik, G. Farrell, D. Liu, V. Kavungal, Q. Wu, and Y. Semenova, "A coated spherical microresonator for measurement of water vapor concentration at PPM levels in very low humidity environments," *J. Lightwave Technol.* **36**, 2667–2674 (2018).
- T. Xing, E. Xing, T. Jia, J. Li, J. Rong, Y. Zhou, W. Liu, J. Tang, and J. Liu, "Fast switching acoustic sensor with ultrahigh sensitivity and wide dynamic response range based on ultrahigh-Q CaF_2 resonator," *J. Lightwave Technol.* **40**, 5775–5780 (2022).
- J. Liao, A. Qavi, M. Adolphson, and L. Yang, "High-Q WGM resonators encapsulated in PDMS for highly sensitive displacement detection," *J. Lightwave Technol.* **41**, 2862–2869 (2023).
- V. Kavungal, G. Farrell, Q. Wu, A. K. Mallik, and Y. Semenova, "A packaged whispering gallery mode strain sensor based on a polymer-wire cylindrical micro resonator," *J. Lightwave Technol.* **36**, 1757–1765 (2018).
- B. Duan, H. Zou, J.-H. Chen, C. H. Ma, X. Zhao, X. Zheng, C. Wang, L. Liu, and D. Yang, "High-precision whispering gallery microsensors with ergodic spectra empowered by machine learning," *Photon. Res.* **10**, 2343–2348 (2022).
- J. Zhu, S. K. Ozdemir, Y.-F. Xiao, L. Li, L. He, D.-R. Chen, and L. Yang, "On-chip single nanoparticle detection and sizing by mode splitting in an ultrahigh-Q microresonator," *Nat. Photonics* **4**, 46–49 (2010).
- L. He, Ş. K. Özdemir, J. Zhu, W. Kim, and L. Yang, "Detecting single viruses and nanoparticles using whispering gallery microlasers," *Nat. Nanotechnol.* **6**, 428–432 (2011).
- H. Xu, M. Hafezi, J. Fan, J. M. Taylor, G. F. Strouse, and Z. Ahmed, "Ultra-sensitive chip-based photonic temperature sensor using ring resonator structures," *Opt. Express* **22**, 3098–3104 (2014).
- J. Wang, Y. Pan, J. Gao, C. Zhang, Z. Qu, T. Xu, Y. Shen, and J. Qu, "An on-chip silicon photonics thermometer with milli-kelvin resolution," *Appl. Sci.* **12**, 3713 (2022).
- J. Liao and L. Yang, "Optical whispering-gallery mode barcodes for high-precision and wide-range temperature measurements," *Light Sci. Appl.* **10**, 32 (2021).
- S. Zhao, Q. Liu, J. Chen, and Z. He, "Resonant fiber-optic strain and temperature sensor achieving thermal-noise-limit resolution," *Opt. Express* **29**, 1870–1878 (2021).
- X. Zhu, Y. Li, Z. Lin, M. You, and J. Liu, "Stability of silicon resonator temperature sensors with the Pound–Drever–Hall technique," *Opt. Lett.* **48**, 924–927 (2023).
- G. Li, L. Ji, G. Li, J. Su, and C. Wu, "High-resolution and large-dynamic-range temperature sensor using fiber Bragg grating Fabry–Pérot cavity," *Opt. Express* **29**, 18523–18529 (2021).
- T. Herr, V. Brasch, J. D. Jost, C. Y. Wang, N. M. Kondratiev, M. L. Gorodetsky, and T. J. Kippenberg, "Temporal solitons in optical microresonators," *Nat. Photonics* **8**, 145–152 (2014).
- Q.-F. Yang, B. Shen, H. Wang, M. Tran, Z. Zhang, K. Y. Yang, L. Wu, C. Bao, J. Bowers, A. Yariv, and K. Vahala, "Vernier spectrometer using counterpropagating soliton microcombs," *Science* **363**, 965–968 (2019).
- R. Niu, M. Li, S. Wan, Y. R. Sun, S.-M. Hu, C.-L. Zou, G.-C. Guo, and C.-H. Dong, "kHz-precision wavemeter based on reconfigurable microsoliton," *Nat. Commun.* **14**, 169 (2023).
- Y. Sun, J. Wu, M. Tan, X. Xu, Y. Li, R. Morandotti, A. Mitchell, and D. J. Moss, "Applications of optical microcombs," *Adv. Opt. Photon.* **15**, 86–175 (2023).
- B.-B. Li, Q.-Y. Wang, Y.-F. Xiao, X.-F. Jiang, Y. Li, L. Xiao, and Q. Gong, "On chip, high-sensitivity thermal sensor based on high-Q polydimethylsiloxane-coated microresonator," *Appl. Phys. Lett.* **96**, 251109 (2010).
- J. Alnis, A. Schliesser, C. Y. Wang, J. Hofer, T. J. Kippenberg, and T. W. Hänsch, "Thermal-noise-limited crystalline whispering-gallery-mode resonator for laser stabilization," *Phys. Rev. A* **84**, 011804 (2011).
- J. D. Swaim, J. Knittel, and W. P. Bowen, "Detection of nanoparticles with a frequency locked whispering gallery mode microresonator," *Appl. Phys. Lett.* **102**, 183106 (2013).

29. W. Weng, J. D. Anstie, T. M. Stace, G. Campbell, F. N. Baynes, and A. N. Luiten, "Nano-Kelvin thermometry and temperature control: beyond the thermal noise limit," *Phys. Rev. Lett.* **112**, 160801 (2014).
30. J. Lim, A. A. Savchenkov, E. Dale, W. Liang, D. Elyahu, V. Ilchenko, A. B. Matsko, L. Maleki, and C. W. Wong, "Chasing the thermodynamical noise limit in whispering-gallery-mode resonators for ultrastable laser frequency stabilization," *Nat. Commun.* **8**, 8 (2017).
31. S. Fujii and T. Tanabe, "Dispersion engineering and measurement of whispering gallery mode microresonator for Kerr frequency comb generation," *Nanophotonics* **9**, 1087–1104 (2020).
32. C. Zhang, G. Kang, J. Wang, Y. Pan, and J. Qu, "Inverse design of soliton microcomb based on genetic algorithm and deep learning," *Opt. Express* **30**, 44395–44407 (2022).
33. K.-N. Joo and S.-W. Kim, "Absolute distance measurement by dispersive interferometry using a femtosecond pulse laser," *Opt. Express* **14**, 5954–5960 (2006).
34. S. Wan, R. Niu, J.-L. Peng, J. Li, G.-C. Guo, C.-L. Zou, and C.-H. Dong, "Fabrication of the high-Q Si_3N_4 microresonators for soliton microcombs," *Chin. Opt. Lett.* **20**, 032201 (2022).
35. C. Zhang, G.-G. Kang, J. Wang, S. Wan, C.-H. Dong, Y.-J. Pan, and J.-F. Qu, "Photonic thermometer by silicon nitride microring resonator with milli-kelvin self-heating effect," *Measurement* **188**, 110494 (2022).
36. Z. Qu, X. Liu, C. Zhang, J. Wang, Y. Wang, Y. Pan, and J. Qu, "Fabrication of an ultra-high quality MgF_2 micro-resonator for a single soliton comb generation," *Opt. Express* **31**, 3005–3016 (2023).
37. J. I. Thorpe, K. Numata, and J. Livas, "Laser frequency stabilization and control through offset sideband locking to optical cavities," *Opt. Express* **16**, 15980–15990 (2008).
38. H. Weng, J. Liu, A. A. Afridi, J. Li, J. Dai, X. Ma, Y. Zhang, Q. Lu, J. F. Donegan, and W. Guo, "Directly accessing octave-spanning dissipative Kerr soliton frequency combs in an AlN microresonator," *Photon. Res.* **9**, 1351–1357 (2021).
39. F. Lei, Z. Ye, and V. Torres-Company, "Thermal noise reduction in soliton microcombs via laser self-cooling," *Opt. Lett.* **47**, 513–516 (2022).
40. L. Stern, A. Naiman, G. Keinan, N. Mazurski, M. Grajower, and U. Levy, "Ultra-precise optical to radio frequency based chip-scale refractive index and temperature sensor," *Optica* **4**, 1–7 (2017).
41. J. Komma, C. Schwarz, G. Hofmann, D. Heinert, and R. Nawrodt, "Thermo-optic coefficient of silicon at 1550 nm and cryogenic temperatures," *Appl. Phys. Lett.* **101**, 041905 (2012).
42. A. W. Elshaari, I. E. Zadeh, K. D. Jons, and V. Zwiller, "Thermo-optic characterization of silicon nitride resonators for cryogenic photonic circuits," *IEEE Photon. J.* **8**, 2701009 (2016).
43. C. Xiang, J. Liu, J. Guo, L. Chang, R. N. Wang, W. Weng, J. Peters, W. Xie, Z. Zhang, J. Riemensberger, J. Selvidge, T. J. Kippenberg, and J. E. Bowers, "Laser soliton microcombs on silicon," *Science* **373**, 99–103 (2021).
44. H. Arianfard, S. Juodkazis, D. J. Moss, and J. Wu, "Sagnac interference in integrated photonics," *Appl. Phys. Rev.* **10**, 011309 (2023).
45. H. Zhang, C. Jiang, X. Zhu, J. Hu, P. Wang, H. Li, S. Sun, and T. Cao, "High-sensitivity transverse-load and axial-strain sensor based on air-bubble Fabry–Pérot cavity and fiber Sagnac loop cascaded," *IEEE Sens. J.* **23**, 5795–5802 (2023).
46. G.-D. Kim, H.-S. Lee, C.-H. Park, S.-S. Lee, B. T. Lim, H. K. Bae, and W.-G. Lee, "Silicon photonic temperature sensor employing a ring resonator manufactured using a standard CMOS process," *Opt. Express* **18**, 22215–22221 (2010).